



1 **Magnetospheric chaos and dynamical complexity response during storm time disturbance**

2 Irewola Aaron Oludehinwa¹, Oluksunkanmi Isaac Oluksola¹, Oluwale Segun Bolaji^{1,2}, Olukside
3 Olayinka Odeyemi¹, Abdullahi Ndzi Njah¹

4 ¹Department of Physics, University of Lagos, Nigeria

5 ²Department of Physics, University of Tasmania, Australia

6 **Abstract**

7 In this study, we examine the magnetospheric chaos and dynamical complexity response in the
8 disturbance storm time (D_{st}) and solar wind electric field (VB_s) during different categories of
9 geomagnetic storm (minor, moderate and major geomagnetic storm). The time series data of the
10 D_{st} and VB_s are analyzed for the period of nine years using nonlinear dynamics tools (Maximal
11 Lyapunov Exponent, MLE, Approximate Entropy, ApEn and Delay Vector Variance, DVV). We
12 found a significant trend between each nonlinear parameter and the categories of geomagnetic
13 storm. The MLE and ApEn values of the D_{st} indicate that chaotic and dynamical complexity
14 response are high during minor geomagnetic storms, reduce at moderate geomagnetic storms and
15 declined further during major geomagnetic storms. However, the MLE and ApEn values obtained
16 in VB_s indicate that chaotic and dynamical complexity response are high with no significant
17 difference between the periods that are associated with minor, moderate and major geomagnetic
18 storms. The test for nonlinearity in the D_{st} time series during major geomagnetic storm reveals the
19 strongest nonlinearity features. Based on these findings, the dynamical features obtained in the
20 VB_s as input and D_{st} as output of the magnetospheric system suggest that the magnetospheric
21 dynamics is nonlinear and the solar wind dynamics is consistently stochastic in nature.

22 **Keywords:** D_{st} signals, Solar wind electric field (VB_s) signals, Geomagnetic storm, Chaotic
23 behaviour, Dynamical complexity, Nonlinearity.

24



25 1.0 Introduction

26 The response of chaos and dynamical complexity behaviour with respect to magnetospheric
27 dynamics varies. This is due to changes in the interplanetary electric fields imposed on the
28 magnetopause and those penetrating the inner magnetosphere and sustaining convection thereby
29 initiating geomagnetic storm (Pavlos et al. 1992). A prolonged southward turning of interplanetary
30 magnetic field (IMF, B_z), which indicates that solar wind-magnetosphere coupling is in-progress
31 was confirmed on many occasions **that** such geomagnetic storm was driven by corona mass
32 ejection (Russell et al. 1974; Burton et al. 1975; Gonzalez and Tsurutani, 1987; Cowley, 1995;
33 Tsutomu, 2002). Irrespective of what causes the geomagnetic storm, the disturbance storm time
34 (D_{st}) remains the most popular global indicator that can precisely unveil the severity of a
35 geomagnetic storm (Dessel and Parker, 1959).

36 **The dynamics in the D_{st} signal displays signature of fluctuations in its underlying dynamics at**
37 **different categories of geomagnetic storm.** Ordinarily, one can easily anticipate that fluctuations
38 in a D_{st} signal appear chaotic and complex. These may arise from the changes in the interplanetary
39 electric fields driven by the solar wind-magnetospheric coupling processes. At different categories
40 of geomagnetic storm, fluctuations in the D_{st} signals differ (Oludehinwa et al. 2018). One obvious
41 reason is that as the intensity of the geomagnetic storm increases, the fluctuation behaviour in the
42 D_{st} signal becomes more complex and nonlinear in nature. ~~It's have~~ been established that the
43 electrodynamic response of the magnetosphere to solar wind ~~driven~~ are non-autonomous in nature
44 (Price and Prichard, 1993; Price et al. 1994; Johnson and Wings, 2005). Therefore, the chaotic
45 analysis of the magnetospheric time series must be related to the concept of input-output dynamical
46 process. Consequently, it is necessary to examine the chaotic behaviour of the solar wind electric



47 field (VB_s) as input signals and the magnetospheric activity index (D_{st}) as output during different
48 categories of geomagnetic storms.

49 Several works have been presented on the chaotic and dynamical complexity behaviour of the
50 magnetospheric dynamics based on autonomous concept, i.e using the time series data of
51 magnetospheric activity alone such as auroral electrojet (AE), lower auroral electrojet (AL) and
52 D_{st} index (Vassilidia et al.1990; Baker and Klimas, 1990; Vassilidia et al.1991; Shan et al. 1991;
53 Pavlos et al. 1994; Klimas et al. 1996; Valdivia et al. 2005; Mendes et al. 2017; Consolini, 2018).
54 They found evidence of low-dimensional chaos in the magnetospheric dynamics. For instance, the
55 report by Vassilidia et al. (1991) shows that the computation of Lyapunov exponent for AL index
56 time series gives a positive value of Lyapunov exponent indicating the presence of chaos in the
57 magnetospheric dynamics. Unnikrishnan, (2008) studied the deterministic chaotic behaviour in the
58 magnetospheric dynamics under various physical conditions using AE index time series and found
59 that the seasonal mean value of Lyapunov exponent in winter season during quiet periods ($0.7 \pm$
60 0.11 min^{-1}) is higher than that of the stormy periods ($0.36 \pm 0.09 \text{ min}^{-1}$). Balasis et al. (2006)
61 examined the magnetospheric dynamics in the D_{st} index time series from pre-magnetic storm to
62 magnetic storm period using fractal dynamics. They found that the transition from anti-persistent
63 to persistent behaviour indicates that the occurrence of an intense geomagnetic storm is imminent.
64 Balasis et al. (2009) further reveal the dynamical complexity behaviour in the magnetospheric
65 dynamics using various entropy measures. They reported a significant decrease in dynamical
66 complexity and an accession of persistency in the D_{st} time series as the magnetic storm
67 approaches. Recently, Oludehinwa et al. (2018) examined the nonlinearity effects in D_{st} signals
68 during minor, moderate and major geomagnetic storm using recurrence plot and recurrence



69 quantification analysis. They found that the dynamics of the D_{st} signal is stochastic during minor
70 geomagnetic storm periods and deterministic as the geomagnetic storm increases.

71 Also, studies describing the solar wind and magnetosphere as non-autonomous system have been
72 extensively investigated. Price et al. (1994) examine the nonlinear input-output analysis of AL
73 index and different combinations of interplanetary magnetic field (IMF) with solar wind
74 parameters as input function. They found that only a few of the input combinations show any
75 evidence whatsoever for nonlinear coupling between the input and output for the interval
76 investigated. Pavlos et al. (1999) extends further evidence of magnetospheric chaos. They
77 compared the observational behaviour of the magnetospheric system with the results obtained by
78 analyzing different types of stochastic and deterministic input-output systems and assert that a low
79 dimensional chaos is evident in magnetospheric dynamics. Devi et al. (2013) studied the
80 magnetospheric dynamics using AL index with the southward component of IMF, (B_z) and
81 observed that the magnetosphere and turbulent solar wind have values corresponding to nonlinear
82 dynamical system with chaotic behaviour. The modeling and forecasting approach have been
83 applied to magnetospheric time series using nonlinear models (Valdivia et al. 1996; Vassiliadis et
84 al. 1999; Vassiliadis, 2006; Balikhin et al. 2010). These efforts have improved our understanding
85 with regards to the facts that nonlinear dynamics can reveal some hidden dynamical information
86 in the observational time series. In addition to these nonlinear effects in D_{st} signals, a measure of
87 the exponential divergence and convergence within the trajectories of a phase space known as
88 (Maximal Lyapunov Exponent, MLE), which have the potential to depicts the chaotic behavior in
89 the D_{st} and VB_s time series during a minor, moderate and major geomagnetic storm have not been
90 investigated. In addition, to the best of our knowledge, computation of Approximate Entropy
91 (ApEn) that depicts the dynamical complexity behaviour during different categories of



92 geomagnetic storm has not been reported in the literature. The test for nonlinearity through delay
93 vector variance (DVV) analysis that establishes the degree at which nonlinearity response in D_{st}
94 time series during minor, moderate and major geomagnetic storms is not well known. It is worth
95 to note that understanding the dynamical characteristics in the D_{st} and VB_s signals at different
96 categories of geomagnetic storms will provide useful diagnostic information to different conditions
97 of space weather phenomenon. Consequently, this study attempts to carry out comprehensive
98 numerical analysis to unfold the chaotic and dynamical complexity behaviour in the D_{st} and VB_s
99 signals during minor, moderate and major geomagnetic storm. In section 2, our methods of data
100 acquisition are described. Also, the nonlinear analysis that we employed in this investigation are
101 detailed. In section 3, we unveiled our results and engage the discussion of results in section 5.

102 2.0 Description of the Data and Nonlinear Dynamics

103 The D_{st} index is a record of ground-based magnetic stations at low-latitudes observatories around
104 the world and depicts the variation of the magnetospheric currents such as the chapman-ferraro
105 current in the magnetopause, ring and tail currents (Sugiura, 1964; Love and Gannon, 2009). Due
106 to its global nature, D_{st} time series provides a measure of how intense a geomagnetic storm was
107 (Dessel and Parker, 1959). In this study, we considered D_{st} data for the period of nine years from
108 January to December between 2008 and 2016 which were downloaded from the World Data Centre
109 for Geomagnetism, Kyoto, Japan (<http://wdc.kugi-kyoto-u.ac.jp/Dstae/index.html>). We use the
110 classification of geomagnetic storms as proposed by Gonzalez et al. (1994) such that D_{st} index
111 value in the ranges $0 \leq Dst \leq -50nT$, $-50nT \leq Dst \leq -100nT$, $-100nT \leq Dst \leq -250nT$
112 are classified as minor, moderate and major geomagnetic storms respectively. The solar wind
113 electric field (VB_s) data are archived from the National Aeronautics and Space Administration,
114 Space Physics Facility (<http://omniweb.gsfc.nasa.gov>). It is well known that the dynamics of the



115 solar wind contribute to the driving of the magnetosphere (Burton et al. 1975). Furthermore, we
116 took the solar wind electric field (VB_s) as the input signals (Price and Prichard, 1993; Price et al.
117 1994). The VB_s was categorized according to the periods of minor, moderate and major
118 geomagnetic storm. Then, the D_{st} and VB_s time series were subjected to a variety of nonlinear
119 analytical tools explained as follow:

120 **2.1 Phase Space Reconstruction and Observational time series**

121 An observational time series can be defined as a sequence of scalar measurements of some
122 quantity, which is a function of the current state of the system taken at multiples of a fixed sampling
123 time. In nonlinear dynamics, the first step in analyzing an observational time series data is to
124 reconstruct an appropriate state space of the system. Takens, (1981) and Mane, (1981) stated that
125 one time series or a few simultaneous time series are converted to a sequence of vectors. This
126 reconstructed phase space has all the dynamical characteristic of the real phase space provided the
127 time delay and embedding dimension are properly specified.

$$128 \quad X(t) = [x(t), x(t + \tau), x(t + 2\tau), \dots, x(t + (m - 1)\tau)]^T \quad (1)$$

129 Where $X(t)$ is the reconstructed phase space, $x(t)$ is the original time series data, τ is the time
130 delay and m is the embedding dimension. An appropriate choice of τ and m are needed for the
131 reconstruction phase space which is determined by average mutual information and false nearest
132 neighbour respectively.

133

134

135



136 2.2 Average Mutual Information (AMI)

137 The method of Average Mutual Information (AMI) is one of the nonlinear techniques used to
138 determine the optimal time delay (τ) required for phase space reconstruction in observational time
139 series. The time delay mutual information was proposed by Fraser and Swinney, (1986) instead of
140 autocorrelation function. This method takes into account nonlinear correlations within the time
141 series data. It measures how much information can be predicted about one time series point, given
142 full information about the other. For instance, the mutual information between x_i and $x_{(i+\tau)}$
143 quantifies the information in state $x_{(i+\tau)}$ under the assumption that information at the state x_i is
144 known. The AMI for a time series, $x(t_i)$, $i = 1, 2, \dots, N$ is calculated as:

$$145 \quad I(T) = \sum_{x(t_i), x(t_i+T)} P(x(t_i), x(t_i + T)) \times \log_2 \left[\frac{P(x(t_i), x(t_i+T))}{P(x(t_i)) P(x(t_i+T))} \right] \quad (2)$$

146 Where $x(t_i)$ is the i th element of the time series, $T = k\Delta t$ ($k = 1, 2, \dots, k_{max}$), $P(x(t_i))$ is the
147 probability density at $x(t_i)$, $P(x(t_i), x(t_i + T))$ is the joint probability density at the pair
148 $x(t_i), x(t_i + T)$. The time delay (τ) of the first minimum of AMI is chosen as optimal time delay
149 (Fraser and Swinney, 1986). Therefore, the AMI was applied to the D_{st} and VB_s time series and
150 the plot of AMI against time delay is shown in Figure (3). We notice that the AMI showed the first
151 local minimum at roughly ($\tau = 15hr$). Furthermore, the values of τ near this value of ($\sim 15hr$)
152 maintain constancy for both VBs and D_{st} . In the analysis ($\tau = 15hr$) was used as the optimal
153 time delay for the computation of maximal Lyapunov exponent.

154

155

156



157 2.3 False Nearest Neighbour (FNN)

158 In determining the optimal choice of embedding dimension(m), the false nearest neighbour
159 method was used in the study. It was suggested by Kennel et al. (1993). The concept is based on
160 how the number of neighbours of a point along a signal trajectory changes with increasing
161 embedding dimension. With increasing embedding dimension, the false neighbour will no longer
162 be neighbours, therefore by examining how the number of neighbours changes as a function of
163 dimension, an appropriate embedding dimension can be determined. The FNN is calculated such
164 that a sequence of vector is reconstructed in the form as

$$165 \quad P(i) = \{X_i, X_{i+\tau}, X_{i+2\tau}, \dots, X_{i+(m-1)\tau}\} \quad (3)$$

166 Where τ is the time delay for each point in the m -dimensional embedding space, after that the
167 algorithm search for neighbour $P(j)$ such that, $|P(i) - P(j)| < \varepsilon$, where ε is a small constant
168 usually of the order of the standard deviation of the time series. Then a normalized distance $\Gamma(i)$
169 between the $(m + 1)$ th embedding coordinates of points $P(i)$ and $P(j)$ can be computed as

$$170 \quad \Gamma(i) = \frac{|X_{i+m\tau} - X_{j+m\tau}|}{|P(i) - P(j)|} \quad (4)$$

171 **If the distance of the iteration to the nearest neighbor ratio** exceeds a defined threshold(ε), the
172 points are considered as false neighbor. In the analysis, the FNN was applied to the D_{st} and VB_s
173 time series to detect the optimal value of embedding dimension(m). Figure (4) shows a sample
174 plot of **FNN** against embedding dimension in one of the months under investigation (other months
175 show similar results, thus for brevity we depict only one of the results). We notice that the false
176 nearest neighbor attains its minimum value at $m \geq 5$ indicating that embedding dimension (m)



177 from $m \geq 5$ are optimal values. Therefore, $m = 5$ was used for the computation of maximal
178 Lyapunov exponent.

179 **2.4 Maximal Lyapunov Exponent (MLE)**

180 The Maximal Lyapunov Exponent (MLE) is one of the most popular nonlinear dynamics tool used
181 for detecting chaotic behaviour in a time series data. It describes how small changes in the state of
182 a system grow at an exponential rate and eventually dominate the behaviour. An important
183 indication of chaotic behavior of a dissipative deterministic system is the existence of a positive
184 Lyapunov Exponent. A positive MLE signifies divergence of trajectories in one direction or
185 expansion of an initial volume in this direction. On the other hand, a negative MLE exponent
186 implies convergence of trajectories or contraction of volume along another direction. Algorithm
187 proposed by Wolf et al. (1985) for estimating MLE is employed to compute the chaotic behavior
188 of the D_{st} and VB_s time series at minor, moderate and major geomagnetic storm. Other methods
189 of determining MLE includes Rosenstein's method, Kantz's method and so on. In this study, the
190 MLE at minor, moderate and major geomagnetic storms periods was computed with $m = 5$ and
191 $\tau = 15hr$ as shown in figures (5 & 6-bar plots) for D_{st} and VB_s . The calculation of MLE is
192 explained as follows: given a sequence of vector $x(t)$, an m -dimensional phase space is formed
193 from the observational time series through embedding theorem as

$$194 \quad \{x(t), x(t + \tau), \dots, x(t + (m - 1)\tau)\} \quad (5)$$

195 Where m and τ are as defined earlier, after reconstructing the observational time series, the
196 algorithm locates the nearest neighbour (in Euclidean sense) to the initial point $\{x(t_0), \dots, x(t_0 +$
197 $(m - 1)\tau\}$ and denote the distance between these two points $L(t_0)$. At a later time t_1 , the initial
198 length will have evolved to length $L'(t_1)$. Then the MLE is calculated as



199
$$\lambda = \frac{1}{t_M - t_0} \sum_{k=1}^M \log_2 \frac{L'(t_k)}{L(t_{k-1})} \quad (6)$$

200 **M** is the total number of replacement steps.

201 **2.5 Approximate Entropy (ApEn)**

202 Approximate Entropy (ApEn) is one of the nonlinear dynamics tools that measure the dynamical
203 complexity in observational time series. The concept was proposed by Pincus, (1991) which
204 provides a generalized measure of regularity, such that it accounts for the logarithm likelihood in
205 the observational time series. For instance, a dataset of length, N , that repeat itself for m points
206 within a boundary will again repeat itself for $m + 1$ points. Because of its computational
207 advantage, ApEn have been widely used in many areas of disciplines to study dynamical
208 complexity (Pincus and Kalman (2004); Pincus and Goldberger (1994); McKinley et al. (2011);
209 Kannathan et al. (2005); Balasis et al. (2009); Shujuan and Weidong, (2010); Moore and Marchant
210 (2017)). The ApEn is computed using the formula below:

211
$$ApEn(m, r, N) = \frac{1}{N-m+1} \sum_{i=1}^{N-m+1} \log C_i^m(r) - \frac{1}{N-m} \sum_{i=1}^{N-m} \log C_i^m(r) \quad (7)$$

212 where $C_i^m(r) = \frac{1}{N-m+1} \sum_{j=1}^{N-m+1} \Theta(r - \|x_i - x_j\|)$ is the correlation integral, m is the embedding
213 dimension and r is the tolerance. To compute the ApEn for the D_{st} and VB_s time series classified
214 as minor, moderate and major geomagnetic storm from 2008 to 2016, we choose ($m = 3, \tau =$
215 $1hr$). We refer the works of Pincus, (1991); Kannathal et al. (2005); and Balasis et al. (2009) to
216 interested readers where all the computational steps regarding ApEn were explained in details.
217 Figures (5 & 6) depict the stem plot of ApEn for D_{st} and (VB_s) from 2008 to 2016.

218



219 2.6 Delay Vector Variance (DVV) analysis

220 The Delay Vector Variance (DVV) is a unified approach in analyzing and testing for nonlinearity
221 in a time series (Gautama et al. 2004; Mandic et al. 2007). The basic idea of the DVV is that, if
222 two delay vectors of a predictable signal are close to each other in terms of the Euclidean distance,
223 they should have similar target. For instance, when a time delay (τ) is embedded into a time series
224 $x(k)$, $k = 1, 2, \dots, N$, then a reconstructed phase space vector is formed which represents a set of
225 delay vectors (DVs) of a given dimension.

$$226 \quad X(k) = [X_{k-m\tau}, \dots, X_{k-\tau}]^T \quad (8)$$

227 Reconstructing the phase space, a set (λ_k) is generated by grouping those DVs that are with a
228 certain Euclidean distance to DVs ($X(k)$). For a given embedding dimension (m), a measure of
229 unpredictability σ^{*2} is computed over all pairwise Euclidean distance between delay vector as

$$230 \quad d(i, j) = \|x(i) - x(j)\| \quad (i \neq j) \quad (9)$$

231 Then, sets $\lambda_k(r_d)$ are generated as the sets which consist of all delay vectors that lie closer to $x(k)$
232 than a certain distance r_d .

$$233 \quad \lambda_k(r_d) = \{x(i) \mid \|x(k) - x(i)\| \leq r_d\} \quad (10)$$

234 For every set $\lambda_k(r_d)$, the variance of the corresponding target $\sigma^{*2}(r_d)$ is

$$235 \quad \sigma^{*2}(r_d) = \frac{\frac{1}{N} \sum_{k=1}^N \sigma_k^2(r_d)}{\sigma_k} \quad (11)$$

236 where $\sigma^{*2}(r_d)$ is target variance against the standardized distance indicating that Euclidean
237 distance will be varied in a manner standardized with respect to the distribution of pairwise
238 distance between DVs. Iterative Amplitude Adjusted Fourier Transform (IAAFT) method is used



239 to generate the surrogate time series (Kugiumtzis, 1999). If the surrogate time series yields DV
240 plots similar to the original time series and the scattered plot coincides with the bisector line, then
241 the original time series can be regarded as linear (Theiler et al. 1992; Gautama et al.2004; Imitaz,
242 2010; Jaksic et al. 2016). On the other hand, if the surrogate time series yield DV plot that is not
243 similar to that of the original time series, then the deviation from the bisector lines indicates
244 nonlinearity. The deviation from the bisector lines grows as a result of the degree of nonlinearity
245 in the observational time series.

$$246 \quad t^{D_{VV}} = \sqrt{\langle (\sigma^{*2}(r_d) - \frac{\sum_{i=1}^N \sigma_{s,i}^{*2}}{N_s}) \rangle} \quad (12)$$

247 where $\sigma_{s,i}^{*2}(r_d)$ is the target variance at the span r_d for the i^{th} surrogate. To carry out the test for
248 nonlinearity in the D_{st} signals, $m = 3$ and $n_d = 3$, the number of reference DVs=200, and number
249 of surrogate, $N_s = 25$ was used in all the analysis. Then we examined the nonlinearity response at
250 minor, moderate and major geomagnetic storm.



251 3.0 Results

252 In this study, D_{st} and VB_s time series from January to December was analyzed for the period of
253 nine years (2008 to 2016) to examine the chaotic and dynamical complexity response in the
254 magnetospheric dynamics during minor, moderate and major geomagnetic storms. Figures (1) &
255 (2), display the samples of fluctuation signatures of D_{st} and VB_s signals classified as (a): minor,
256 (b): moderate and (c): major geomagnetic storm. The plot of Average Mutual information against
257 time delay (τ) shown in Figure (3) depicts that the first local minimum of the AMI function was
258 found to be roughly $\tau = 15\text{hr}$. Furthermore, we notice that the values of τ near this value of ($\sim 15\text{hr}$)
259 maintain constancy for both VB_s and D_{st} . Also, in figure (4), we display the plot of false nearest
260 neighbour against embedding dimension (m). It is obvious that a decrease in false nearest
261 neighbour when increasing the embedding dimension drop steeply to zero at the optimal
262 dimension ($m = 5$), thereafter the false neighbours stabilizes at that $m = 5$ for VB_s and D_{st} .
263 Therefore, $m = 5$ and $\tau = 15\text{hr}$ was used for the computation of MLE at different categories of
264 geomagnetic storm, while $m = 3$ and $\tau = 1\text{hr}$ are applied for the computation of ApEn values.

265 The results of MLE (bar plot) and ApEn (stem plot) for D_{st} at minor, moderate and major
266 geomagnetic storms are shown in Figure 5. During minor geomagnetic storms, we notice that the
267 value of MLE ranges between 0.07 and 0.14 for most of the months classified as minor
268 geomagnetic storm. Similarly, the ApEn (stem plot) ranges between 0.59 and 0.83 for most of the
269 months categorized as minor geomagnetic storm. It is obvious that strong chaotic behaviour with
270 high dynamical complexity are associated with minor geomagnetic storms. During moderate
271 geomagnetic storm, (see b part of figure 5), we observe a reduction in MLE values (0.04~0.07)
272 compared to minor geomagnetic storm periods. Within the observed values of MLE during
273 moderate geomagnetic storms, we found a slight rise of MLE in the following months (Mar 2008),



274 (Apr 2011), (Jan 2012, Feb 2012, Apr 2012), (Jul 2015, Aug 2015, Sept 2015, Oct2015, Nov 2015)
275 and (Nov 2016). Also, the ApEn revealed a reduction in values between 0.44 and 0.57 at moderate
276 geomagnetic storms. The lowest values of ApEn were noticed in the following months: May 2010,
277 Mar 2011, and Jan 2016. During major geomagnetic storm as shown in Figure 5, the minimum
278 and maximum value of MLE is respectively 0.03 and 0.04 implying a very strong reduction of
279 chaotic behaviour compared with minor and moderate geomagnetic storm. The lowest values of
280 MLE were found in the months of Jul 2012, Jun 2013 and Mar 2015. Interestingly, further
281 reduction in ApEn value (0.29~0.40) was as well noticed during this period. Thus, during major
282 geomagnetic storm, chaotic behaviour and dynamical complexity subsides significantly.

283 We display in Figure 6, the results of MLE and ApEn computation for the VB_s which has been
284 categorized according to the periods of minor, moderate and major geomagnetic storm. The values
285 of MLE (bar plot) were between 0.06 and 0.20 for VB_s . The result obtained indicate strong chaotic
286 behaviour with no significant difference in chaoticity during minor, moderate and major
287 geomagnetic storm. Similarly, the results obtained from computation of ApEn (stem plot) for VB_s
288 depict a minimum value of 0.60 and peak value of 0.87 as shown in Figure 6. The ApEn values of
289 VB_s indicates high dynamical complexity response with no significant difference during the
290 periods of the three categories of geomagnetic storm investigated.

291 The test for nonlinearity in the D_{st} signals during minor, moderate and major geomagnetic storms
292 was analyzed through the DVV analysis. Shown in Figure 9 is the DVV plot and DVV scatter plot
293 during minor geomagnetic storm for January 2009 and January 2014. We found that the DVV
294 plots during minor geomagnetic storms reveals a slight separation between the original and
295 surrogate data. Also, the DVV scatter plots shows a slight deviation from the bisector line between
296 the original and surrogate data which implies nonlinearity. Also, during moderate geomagnetic



297 storm, we notice that the DVV plot depicts a wide separation between the original and the surrogate
298 data. Also, a large deviation from the bisector line between the original and the surrogate data was
299 also noticed in the DVV scatter plot as shown in Figure (8) thus indicating nonlinearity. In Figure
300 (9), we display samples of DVV plot and DVV scatter plot during major geomagnetic storm for
301 Oct 2011 and Dec 2015. The original and the surrogate data showed a very large separation in the
302 DVV plot during major geomagnetic storm. While the DVV scatter plot depict the greatest
303 deviation from the bisector line between the original and the surrogate data which is also an
304 indication of nonlinearity.

305 **4.0 Discussion of Results**

306 **4.1 The chaotic and dynamical complexity response in D_{st} at minor, moderate and major** 307 **geomagnetic storms**

308 Our result shows that the values of MLE for D_{st} during minor geomagnetic storm are prevalent,
309 indicating significant chaotic response during minor geomagnetic stormy periods (bar plot, Figure
310 5). This increase in chaotic behaviour for D_{st} signals during minor geomagnetic storm may be as
311 a result of asymmetry features in the longitudinal distribution of solar source region for the CMEs
312 signatures responsible for the development of geomagnetic storms (Zhang et al., 2002; Watari,
313 2017). Therefore, we suspect that the increase in chaotic behaviour during minor geomagnetic
314 storm is strongly associated with the longitudinal distribution of solar source region for CMEs.

315 For most of these periods of moderate geomagnetic storms, the values of MLE decreases compared
316 to minor geomagnetic storms. This revealed that as geomagnetic stormy events build up, the level
317 of unpredictability and sensitive dependence on initial condition (chaos) begin to decrease
318 (Lorentz, 1963; Stogatz, 1994). The chaotic behaviour during major geomagnetic storm decreases
319 significantly compared with moderate geomagnetic storm. The reduction in chaotic response



320 during moderate and its further declines at major geomagnetic storm may be attributed to the
321 disturbance in the interplanetary medium driven by solar corona mass ejection (CMEs) or co-
322 rotating interaction region of the solar wind with the magnetosphere (Tsurutani et al. 2003).
323 Notably, the dynamics of the solar wind-magnetospheric interaction are dissipative chaotic in
324 nature (Pavlos, 2012); and, the electrodynamic of the magnetosphere due to the flux of
325 interplanetary electric fields had a significant impact on the state of the chaotic signatures. For
326 instance, the observation of strong chaotic behaviour during minor geomagnetic storm suggests
327 that the dynamics was characterized by a weak magnetospheric disturbance. While the reduction
328 in chaotic behaviour at moderate and major geomagnetic storm period reveals the dynamical
329 features with regards to when a strong magnetospheric disturbance begins to emerge. Therefore,
330 our observation of chaotic signatures at different categories of geomagnetic storm has potential
331 capacity to give useful diagnostic information about **impending** space weather events. It is
332 important to note that the features of D_{st} chaotic behaviour at different categories of geomagnetic
333 storm has not been reported in the literature. For example, previous study of Balasis et al. (2009,
334 2011) investigate dynamical complexity behaviour using different entropy measures and revealed
335 the existence of low dynamical complexity in the magnetospheric dynamics and attributed it to
336 ongoing large magnetospheric disturbance (major geomagnetic storm). The work of Balasis et al.
337 (2009, 2011) where certain dynamical characteristic evolved in the D_{st} signal was revealed was
338 limited to one year data (2001). It is worthy to note that the year 2001, according to sunspot
339 variations is a period of high solar activity during solar cycle 23. It is characterized by numerous
340 and strong solar eruptions that were followed by significant magnetic storm activities. This
341 confirms that on most of the days in year 2001, the geomagnetic activity is strongly associated
342 with major geomagnetic storm. The confirmation of low dynamical complexity response in the D_{st}



343 signal during major geomagnetic storm agree with our current study. However, the idea of
344 comparing the dynamical complexity behaviour at different categories of geomagnetic storm and
345 reveal its chaotic features was not reported. This is the major reason why our present investigation
346 is crucial to the understanding of the level of chaos and dynamical complexity involved during
347 different categories of geomagnetic storm. As an **extension to a year investigation** done by Balasis
348 et al. (2009, 2011) during a major geomagnetic storm, we further investigated nine years data of
349 D_{st} that covered minor, moderate and major geomagnetic storm (see figure 5, stem plots) and
350 unveiled their dynamical complexity behaviour. During major geomagnetic stormy periods, we
351 found that the ApEn values decrease significantly, indicating reduction in the dynamical
352 complexity behaviour. This is in agreement with the low dynamical complexity reported by Balasis
353 et al. (2009, 2011) during a major geomagnetic period. Finally, based on the method of DVV
354 analysis, we found that test of nonlinearity in the D_{st} time series during major geomagnetic storm
355 reveals the strongest nonlinearity features.

356 **4.2 The chaotic and dynamical complexity behaviour in the VB_s as input signals.**

357 The results of the MLE values for VB_s revealed a strong chaotic behaviour during the three
358 categories of geomagnetic storm. Comparing these MLE values during minor to those observed
359 during moderate and major geomagnetic storm, the result obtained did not indicate any significant
360 difference in chaoticity (bar plots, Figure 6). Also, the ApEn values of VB_s during the periods
361 associated with minor, moderate and major geomagnetic storm revealed high dynamical
362 complexity behaviour with no significant difference between the three categories of geomagnetic
363 storm investigated. These observation of high chaotic and dynamical complexity behaviour in the
364 dynamics of VB_s may be due to interplanetary discontinuities **cause** by the abrupt changes in the
365 interplanetary magnetic field direction and plasma parameters (Tsurutani et al. 2010). Also, the



366 indication of high chaotic and dynamical complexity behaviour in VB_s signifies that the solar wind
367 electric field is stochastic in nature. It is worth mentioning that the dynamical complexity
368 behaviour for VB_s is different from what was observed for D_{st} time series data. For instance, our
369 results for D_{st} times series revealed that the chaotic and dynamical complexity behaviour of the
370 magnetospheric dynamics are high during minor geomagnetic storm, reduce at moderate
371 geomagnetic storm and further decline during major geomagnetic storm. While the VB_s signal
372 revealed a high chaotic and dynamical complexity behaviour at all the categories of geomagnetic
373 storm period. Therefore, these dynamical features obtained in the VB_s as input signal and the D_{st}
374 as the output in describing the magnetosphere as a non-autonomous system further support the
375 finding of Donner et al. (2019) that found increased or not changed in dynamical complexity
376 behaviour for VB_s and low dynamical complexity behaviour during storm using recurrence
377 method. Thus, suggesting that the magnetospheric dynamics is nonlinear and the solar wind
378 dynamics is consistently stochastic in nature.

379 **5.0 Conclusions**

380 This work has examined the magnetospheric chaos and dynamical complexity behaviour in the
381 disturbance storm time (D_{st}) and solar wind electric field (VB_s) as input during different categories
382 of geomagnetic storm. The chaotic and dynamical complexity behaviour at minor, moderate and
383 major geomagnetic storm for solar wind electric field (VB_s) as input and D_{st} as output of the
384 magnetospheric system were analyzed for the period of 9 years using nonlinear dynamics tools.
385 Our analysis has shown a noticeable trend of these nonlinear parameters (MLE and ApEn) and the
386 categories of geomagnetic storm (minor, moderate and major). The MLE and ApEn values of the
387 D_{st} have indicated that the chaotic and dynamical complexity behaviour are high during minor
388 geomagnetic storm, low during moderate geomagnetic storm and further reduced during major



389 geomagnetic storm. The values of MLE and ApEn obtained from VB_s indicate that chaotic and
390 dynamical complexity are high with no significant difference during the periods of minor,
391 moderate and major geomagnetic storm. Finally, the test for nonlinearity in the D_{st} time series
392 during major geomagnetic storm reveals the strongest nonlinearity features. Based on these
393 findings, the dynamical features obtained in the VB_s as input and D_{st} as output of the
394 magnetospheric system suggest that the magnetospheric dynamics is nonlinear and the solar wind
395 dynamics is consistently stochastic in nature.

396 **7.0 Acknowledgement**

397 The authors would like to acknowledge the World Data Centre for Geomagnetism, Kyoto, and the
398 National Aeronautics and Space Administration, Space Physics Facility (NASA) for making the
399 Dst data and solar wind plasma data available for research purpose.

400 **Declaration of Interest statement**

401 The authors declare that there is no conflicts of interest.

402

403

404

405

406

407

408

409

410

411



412 **References**

- 413 Baker, D.N., Klimas, A.J., (1990). The evolution of weak to strong geomagnetic activity: An
414 interpretation in terms of deterministic chaos. *J. Geophys. Res. Letts.* Vol. 17, No. 1, PP. 41-
415 44.
- 416 Balasis, G., Daglis, I.A., Anastasiadia, A., Eftaxias, K., (2011). Detection of dynamical complexity
417 changes in Dst time series using entropy concepts and rescaled range analysis. W.Liu, M.
418 Fujimoto (eds.), *The Dynamics Magnetosphere*, IAGA Special Sopron Book Series 3, doi:
419 10.1007/978-94-007-0501-2_12, Springer Science+Business Media B.V. 2011.
- 420 Balasis, G., I.A. Daglis, C. Papadimitriou, M. Kalimeri, A. Anastasiadis, K. Eftaxias (2009).
421 Investigating dynamical complexity in the magnetosphere using various entropy measures,
422 *J.Geophys.Res.*, 114, A0006, doi: 10.1029/2008JA 014035.
- 423 Balasis, G., I.A. Daglis, P. Kaperis, M.Mandea, D. Vassiliadis, K. Eftaxias (2006). From pre-storm
424 activity to magnetic storms: a transition described in terms of fractal dynamics, *Ann.Geophys.*,
425 24, 3557-3567, www.ann-geophys.net/24/3557/2006.
- 426 Balikhin, M.A., Boynton, R.J., Billings, S.A., Gedalin, M., Ganushkina, N., Coca, D., (2010). Data
427 based quest for solar wind-magnetosphere coupling function, *Geophys.Res.Lett.*, 37, L24107,
428 doi: 10.1029/2010GL045733.
- 429 Burton, R.K., McPherron, R.L., Russell, C.T., (1975). An empirical relationship between
430 interplanetary conditions and Dst. *Journal of Geophysical Research*, Vol.80, No.31.



- 431 Consolini, G., (2018), Emergence of dynamical complexity in the Earth's magnetosphere, Machine
432 learning techniques for space weather, PP. 177-202, doi: 10.1016/B978-0-12-811788-0.00007-
433 X
- 434 Cowley, S.W.H., (1995). The earth's magnetosphere: A brief beginner's guide, EOS
435 Trans.Am.GeoPhys.Union, 76, 525.
- 436 Dessler, A.J., Parker, E.N., (1959). Hydromagnetic theory of magnetic storm. J. GeoPhys. Res, 64,
437 PP 2239-2259.
- 438 Devi, S.P., Singh, S.B., Sharma, A.S., (2013). Deterministic dynamics of the magnetosphere:
439 results of the 0-1 test. Nonlin. Processes Geophys., 20, 11-18, 2013, [www.nonlin-processes-](http://www.nonlin-processes-geophys.net/20/11/2013)
440 [geophys.net/20/11/2013](http://www.nonlin-processes-geophys.net/20/11/2013), doi: 10. 5194/npg-20-11-2013.
- 441 Donner, R.V., Balasis, G., Stolbova,V., Georgiou, M., Weideman, M., Kurths, J. (2019).
442 Recurrence-based quantification of dynamical complexity in the earth's magnetosphere at
443 geospace storm time scales. Journal of Geophysical Research: Space Physics, 124, 90-108,
444 doi: 10.1029/2018JA025318.
- 445 Echer, E., Gonzalez, D., Alves, M.V., (2006). On the geomagnetic effects of solar wind
446 interplanetary magnetic structures. Space Weather, Vol.4, S06001,
447 doi:10.1029/2005SW000200.
- 448 Fraser, A.M., (1986). Using mutual information to estimate metric entropy, dimension and
449 entropies in chaotic system, Springer-Verlag, 1986, PP: 82-91.
- 450 Fraser, A.M., Swinney, H.L., (1986). Independent coordinates for strange attractors from mutual
451 information, Phys.Rev.A 33, 1134-1140.



- 452 Gautama, T., Mandic, D.P., Hulle, M.M.V., (2004). The delay vector variance method for detecting
453 determinism and nonlinearity in time series. *Physica D*, 190, 167-176, doi:
454 10.1016/j.physd.2003.11.001.
- 455 Gonzalez, W.D., Joselyn, J.A., Kamide, Y., Kroehl, H.W., Rostoker, G., Tsurutani, B.T.,
456 Vasyliunas, V.M., (1994). What is a geomagnetic storm? *J. Geophys. Res.: Space Physics*,
457 Vol. 99, issue A4, pg. 5771-5792, doi: 10.1029/93JA02867.
- 458 Gonzalez, W.D., Tsurutani, B.T., (1987). Criteria of interplanetary parameters causing intense
459 magnetic storm ($Dst < -100nT$). *Planetary and Space Science*,
460 <https://ntrs.nasa.gov/search.jsp?R=198800068>.
- 461 Horne, R.H., Glauert, S.A., Meredith, N.P., Boscher, D., Maget, V., Heynderickx, D., and Pitford,
462 D. (2013). Space weather impacts on satellites and forecasting the Earth's electron radiation
463 belts with SPACECAST. *Space weather*, **11**, 169 - 186
- 464 Imtiaz, A., (2010). Detection of nonlinearity and stochastic nature in time series by delay vector
465 variance method, *International journal of Engineering & Technology*, Vol. 10, No. 02.
- 466 Jaksic, V., Mandic, D.P., Ryan, K., Basu, B., Pakrashi V., (2016). A Comprehensive Study of the
467 Delay Vector Variance Method for Quantification of Nonlinearity in dynamical Systems.
468 *R.Soc.OpenSci.*, 2016: 3:150493, <http://dx.doi.org/10.1098/rsos.150493>.
- 469 Johnson, J.R., Wing, S., (2005), A solar cycle dependence of nonlinearity in magnetospheric
470 activity. *J. Geophys. Res.*, 110, A04211, doi: 10.1029/2004JA010638.



- 471 Kannathal, N., M.L. Choo, U. R. Acharya, P. K. Sadasivan (2005). Entropies for detecting of
472 epilepsy in EEG, *Computer Methods and Programs in Biomedicine* (2005) 80, 187-194,
473 www.intl.elsevierhealth.com/journals/cmpb.
- 474 Kennel, M.B., R. Brown, H.D.I. Abarbanel (1992). Determining embedding dimension for phase-
475 space reconstruction using a geometrical construction, *PHYSICAL REVIEW A*, Volume 45,
476 Number 6.
- 477 Klimas, A.J., Vassiliadis, D., Baker, D.N., Roberts, D.A., (1996). The organized nonlinear
478 dynamics of the magnetosphere. *J. GeoPhys. Res.* Vol.101, No. A6, PP 13089-13113.
- 479 Kugiumtzis, D., (1999). Test your surrogate before you test your nonlinearity, *Phys. Rev. E*, 60,
480 2808-2816.
- 481 Lorenz, E.N., (1963). Determining nonperiodic flow. *J. Atmos.Sci.*,20,130.
- 482 Love, J.J., Gannon, J.L. (2009). Revised Dst and the epicycles of magnetic disturbance: 1958-2007.
483 *Ann.GeoPhys.*, 27, 3101-3131.
- 484 Mandic, D.P., Chen, M., Gautama, T., Van Hull, M.M., Constantinides, A., (2007). On the
485 Characterization of the Deterministic/Stochastic and Linear/Nonlinear Nature of Time Series.
486 *Proc.R.Soc*, 2008: A464, 1141-1160, doi: 10.1098/rspa. 2007.0154.
- 487 Mane, R., (1981). On the dimension of the compact invariant sets of certain nonlinear maps, D.Rand
488 and L.S.Young, eds, 1981.
- 489 Mckinley, R.A., McIntire, L.K., Schmidt, R., Repperger, D.W., Caldwell, J.A., (2011). Evaluation
490 of Eye Metrics as a Detector of Fatigue. *Human factor*, 53 (4): 403-414, doi:
491 10.1177/0018720811411297.



- 492 Mendes, O., Dominques, M.O., Echer, E., Hajra, R., Menconi, V.E., (2017), Characterization of
493 high-intensity, long-duration continuous auroral activity (HILDCAA) events using
494 recurrence quantification analysis. *Nonlin. Processes Geophys.*,24,407-417, doi:10.5194/npg-
495 24-407-2017.
- 496 Millan, H., Gharbarian-Alavijeh, B., Garcia-Fornaris, I., (2010). Nonlinear dynamics of mean daily
497 temperature and dewpoint time series at Babolsar, Iran, 1961-2005. Elsevier, *Atmospheric*
498 *Research* 98 (2010) 89-101, doi: 10.1016/j.atmosres.2010.06.001.
- 499 Moore, C., Marchant, T., (2017). The approximate entropy concept extended to three dimensions
500 for calibrated, single parameter structural complexity interrogation of volumetric images.
501 *Physics in Medicine & Biology*, 62(15).
- 502 Oludehinwa, I.A., Olusola, O.I., Bolaji, O.S., Odeyemi, O.O., (2018). Investigation of nonlinearity
503 effect during storm time disturbance, *Adv. Space. Res.*, 62 (2018) 440-456, doi:
504 10.1016/j.asr.2018.04.032.
- 505 Omkar, P.T., Verma, P.L., (2013). Solar features and solar wind plasma parameters with
506 geomagnetic storms during the period of 2002-2006. *Indian Journal of Applied Research*,
507 Vol.3, Issue.5, ISSN-2249-555X.
- 508 Pavlos, G.P., (1994). The magnetospheric chaos: a new point of view of the magnetospheric
509 dynamics. Historical evolution of magnetospheric chaos hypothesis the past two decades.
510 Conference Proceeding of the 2nd Panhellenic Symposium held in Democritus University of
511 Thrace, Greece, 26-29, April, edited 1994.
- 512 Pavlos, G.P., (2012). Magnetospheric dynamics and Chaos theory



- 513 Pavlos, G.P., Athanasiu, M.A., Diamantidis, D., Rigas, A.G., Sarri, E.T., (1999). Comments and
514 new results about the magnetospheric chaos hypothesis. *Nonlinear Processes in Geophysics*
515 (1999) 6: 99-127.
- 516 Pavlos, G.P., Rigas, A.G., Dialetis, D., Sarris, E.T., Karakatsanis, L.P., Tsonis, A.A., (1992).
517 Evidence of chaotic dynamics in the outer solar plasma and the earth magnetosphere. *Chaotic*
518 *dynamics: Theory and Practice*, Edited by T. Bountis, Plenum Press, New York, Page. 327-
519 339, doi:10.1007/978-1-4615-3464-8_30.
- 520 Pincus, S.M., (1991). Approximate entropy as a measure of system complexity,
521 *Proc.Natl.Acad.Sci. USA*, Vol.88, PP. 2297-2301.
- 522 Pincus, S.M., Goldberger, A.L., (1994). Physiological time series analysis: what does regularity
523 quantify, *The American Journal of Physiology*, 266 (4): 1643-1656.
- 524 Pincus, S.M., Kalman, E.K., (2004). Irregularity, volatility, risk, and financial market time series,
525 *Proceedings of the National Academy of Sciences*, 101 (38): 13709-13714, doi:
526 10.1073/pnas.0405168101.
- 527 Price, C.P., Prichard, D., Bischoff, J.E., (1994). Nonlinear input/output analysis of the auroral
528 electrojet index. *Journal of Geophysical Research*, Vol.99, No: A7, PP: 227-238.
- 529 Price,C.P., Prichard, D., (1993). The Non-linear response of the magnetosphere: 30 October, 1978.
530 *Geophysical Research Letters*, Vol.20.
- 531 Russell, C.T., (2001). Solar wind and Interplanetary Magnetic Field: A Tutorial. *Space Weather*,
532 *Geophysical Monograph* 125, Page: 73-89.



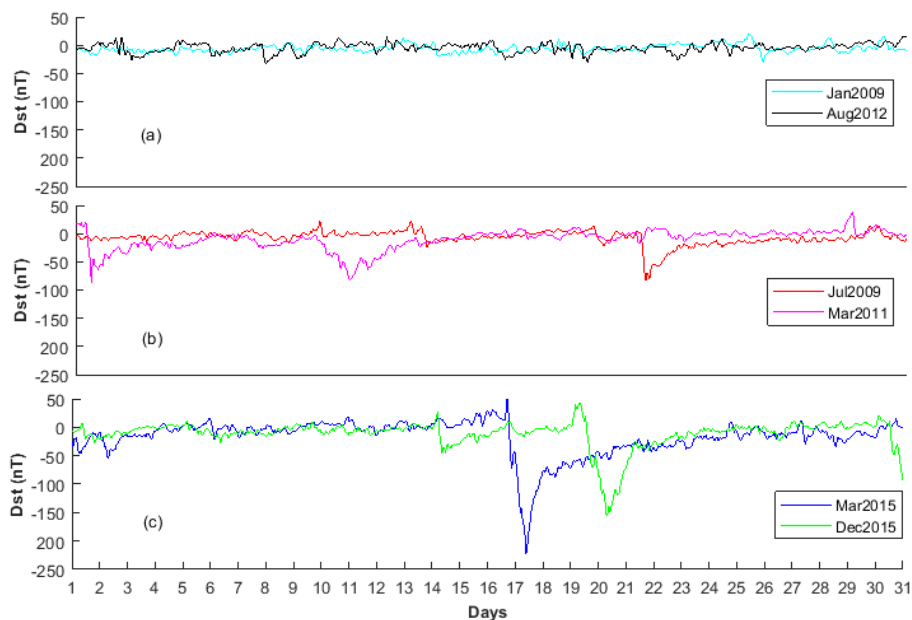
- 533 Russell, C.T., McPherron, R.L., Burton, R.K. (1974). On the cause of geomagnetic storms,
534 J.GeoPhys.Res., 79, 1105-1109.
- 535 Shujuan G., Weidong, Z., (2010). Nonlinear feature comparison of EEG using correlation
536 dimension and approximate entropy, 3rd international conference on biomedical engineering
537 and informatics.
- 538 Strogatz, S.H., (1994), Nonlinear dynamics and chaos with Application to physics, Biology,
539 chemistry and Engineering, New York, John Wiley & Sons.
- 540 Sugiura, M. (1964). Hourly Values of equatorial Dst for the IGY, Ann.Int. GeoPhys. Year, 35, 9-
541 45.
- 542 Takens, F., (1981). Detecting Strange Attractors in Turbulence in Dynamical Systems, *D.Rand &*
543 *L.Young Eds*, 1981: 898, 366-381.
- 544 Theiler, J., Eubank, S., Longtin, A., Galdrikian, B., Farmer, J.D., (1992), Testing for nonlinearity
545 in time series: The method of surrogate data, *Physica D*, 58, 77.
- 546 Tsurutani, B.T., Gonzalez, W.D., Lakhina, G.S. Alex, S., (2003). The extreme magnetic storm of
547 1-2 September 1859, *J. Geophys. Res.* 108(A7), doi: 10.1029/2002JA009504.
- 548 Tsurutani, B.T., Lakhina, G.S., Verkhoglyadova, O.P., Gonzalez, W.D., Echer, E., Guarnieri, F.L.,
549 (2010). A review of interplanetary discontinuities and their geomagnetic effects. *Journal of*
550 *Atmospheric and Solar-Terrestrial Physics*, doi: 10.1016/j.jastp.2010.04.001.
- 551 Tsutomu, N., (2002). Geomagnetic storms. *Journal of communications Research Laboratory*, Vol.
552 49, No.3.



- 553 Unikrishnan, K., (2008). Comparison of chaotic aspect of magnetosphere under various physical
554 conditions using AE index time series. *Ann. Geophys.*, 26, 941-953, [www.ann-
555 geophys.net/26/941/2008](http://www.ann-geophys.net/26/941/2008).
- 556 Unikrishnan, K., Ravindran, S., (2010). A study on chaotic behaviour of equatorial/low latitude
557 ionosphere over indian sub-continent, using GPS-TEC time series, *J. Atmos. Sol. Ter. Phys.*,
558 72, 1080-1089.
- 559 Valdivia, J.A., Rogan, J., Munoz, V., Gomberoff, L., Klimas, A., Vassiliadis, D., Uritsky, V.,
560 Sharma, S., Toledo, B., Wastaviono, L. (2005). The magnetosphere as a complex system. *Adv.
561 Space. Res*, 35, 961-971.
- 562 Valdivia, J.A., Sharma, A.S., Papadopoulos, K., (1996). Prediction of magnetic storms by nonlinear
563 models. *Geophysical Research Letters*, 23(21), 2899-2902, doi: 10.1029/96GL02828.
- 564 Vassiliadis, D., (2006). Systems theory for geospace plasma dynamics, *Rev.Geophys.*, 44, RG2002,
565 doi: 10.1029/2004RG000161.
- 566 Vassiliadis, D., Klimas, A.J., Valdivia, J.A., Baker, D.N., (1999). The geomagnetic response as a
567 function of storm phase and amplitude and solar wind electric field. *Journal of Geophysical
568 Research*, 104(A11), 24957-24976, doi: 10.1029/1999JA900185.
- 569 Vassiliadis, D., Sharma, A.S., Papadopoulos, K., (1991). Lyapunov exponent of magnetospheric
570 activity from AL time series. *J. GeoPhys. Letts*, Vol. 18, No.8, PP. 1643-1646.
- 571 Vassiliadis, D.V., Sharma, A.S., Eastman, T.E., Papadopoulou, K., (1990). Low-dimensional
572 chaos in magnetospheric activity from AE time series. *J. GeoPhys.Res.Lett*, 17, 1841-1844.

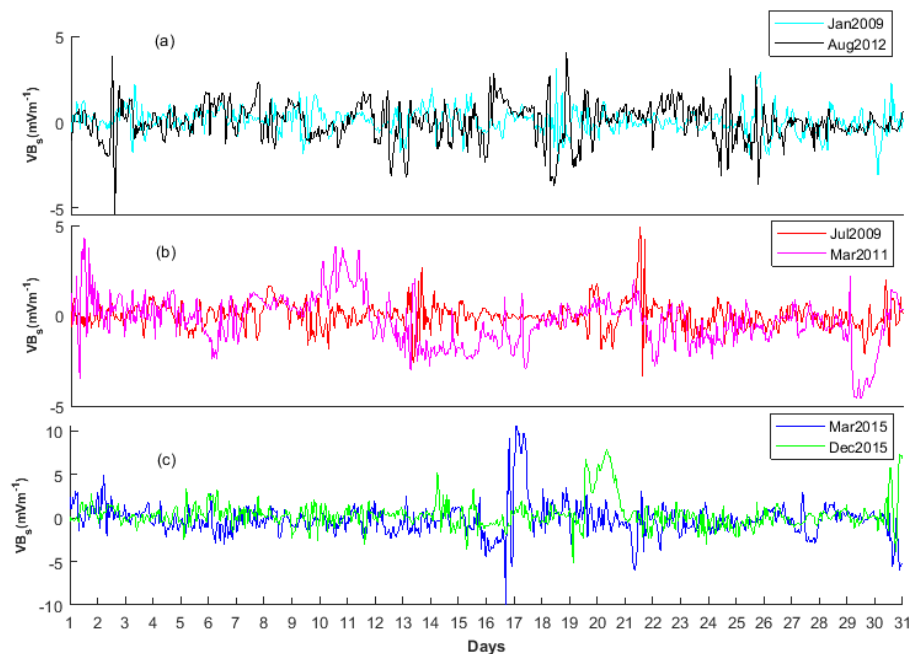


- 573 Watari, S., (2017). Geomagnetic storms of cycle 24 and their solar sources, *Earth, Planets and*
574 *Space*, PP: 69:70, doi: 10.1186/s40623-017-0653-z.
- 575 Wolf, A., Swift, J. B., Swinney, H. L., and Vastano, J. A. (1985). Determining Lyapunov exponents
576 from a time series, *Physica D*, 16, 285–317, doi:10.1016/0167-2789(85)90011-9.
- 577 Zhang, J., Dere, K.P., Howard, R.A., Bothmer, V., (2002), Identification of solar sources of major
578 geomagnetic storms between 1996 and 2000. *Astrophysical Journal*, 582:520-533.



579

580 Figure 1: Samples of Dst signals classified as (a) Minor, (b) Moderate and (c) Major geomagnetic
581 storm

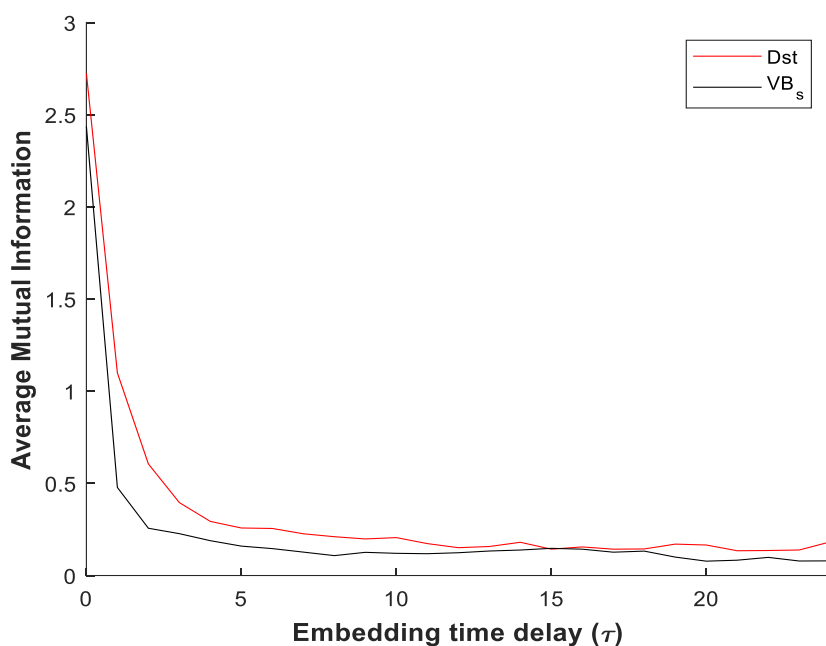


582

583 Figure 2: Samples of (VB_s) during (a) Minor, (b) Moderate and (c) Major geomagnetic storm
584 period.

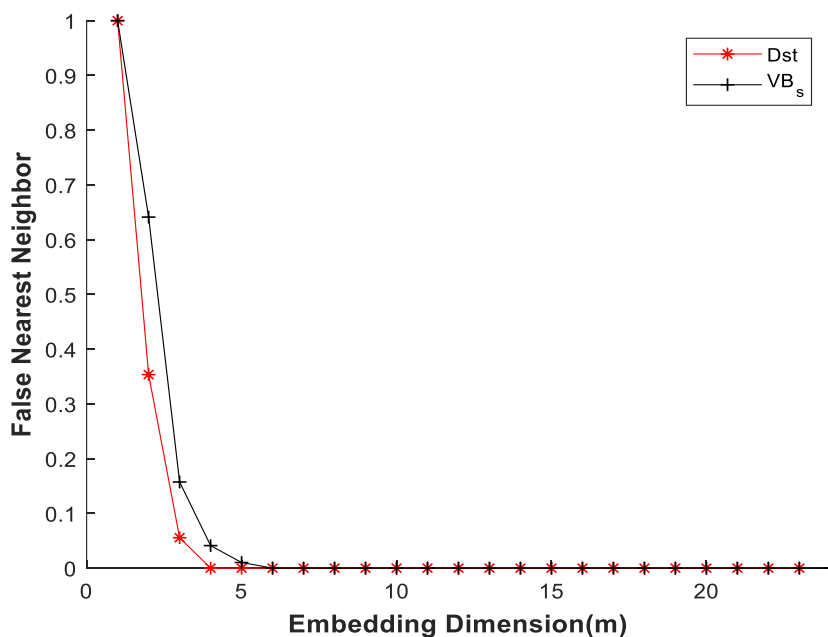


585



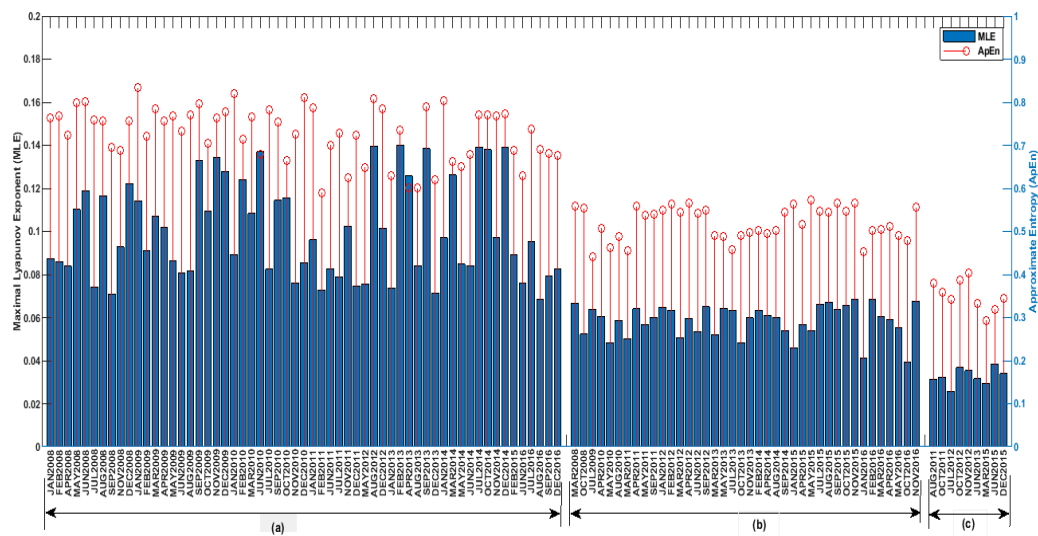
586

587 Figure 3: The plot AMI against embedding time delay (τ)



588

589 Figure 4: The plot of FNN against embedding dimension (m)



590

591 Figure 5: The MLE (bar plot) and ApEn (stem plot) of Dst at: (a) Minor, (b) Moderate and (c)
592 Major geomagnetic storm

593

594

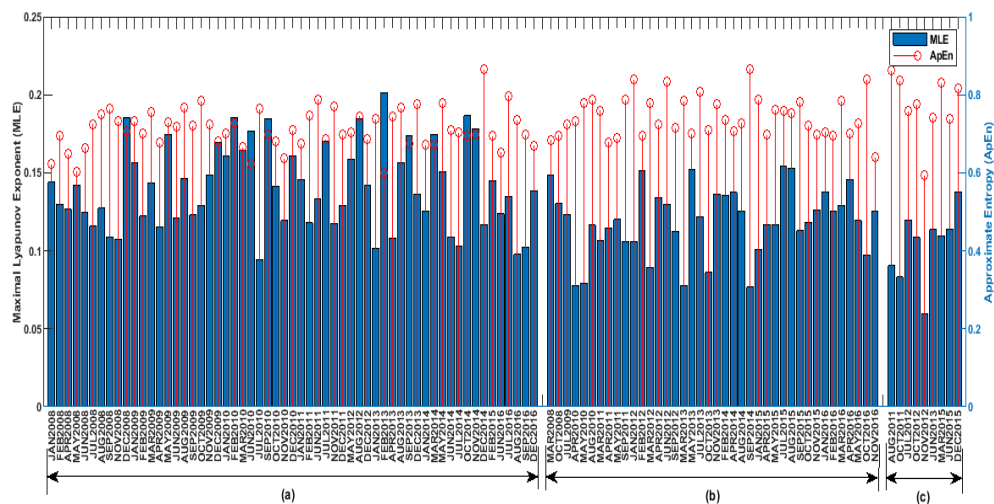
595

596

597

598

599



600

601 Figure 6: The MLE (bar plot) and ApEn (stem plot) of solar wind electric field (VB_s) during: (a)
602 Minor, (b) Moderate and (c) Major geomagnetic storm

603

604

605

606

607

608

609

610

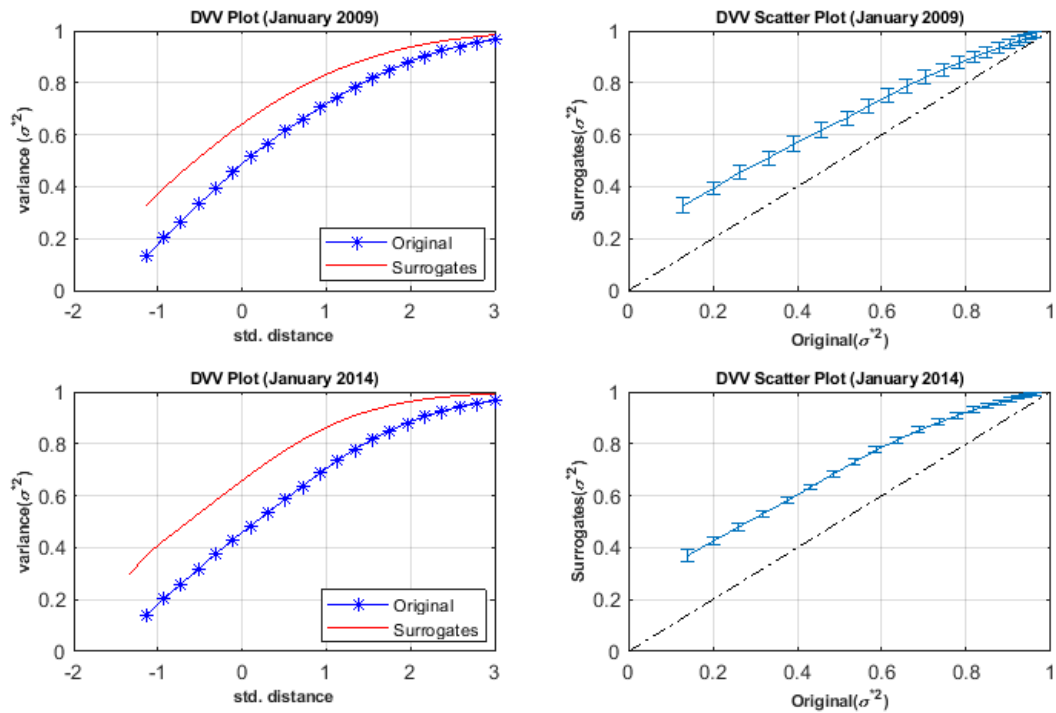
611

612

613

614

615

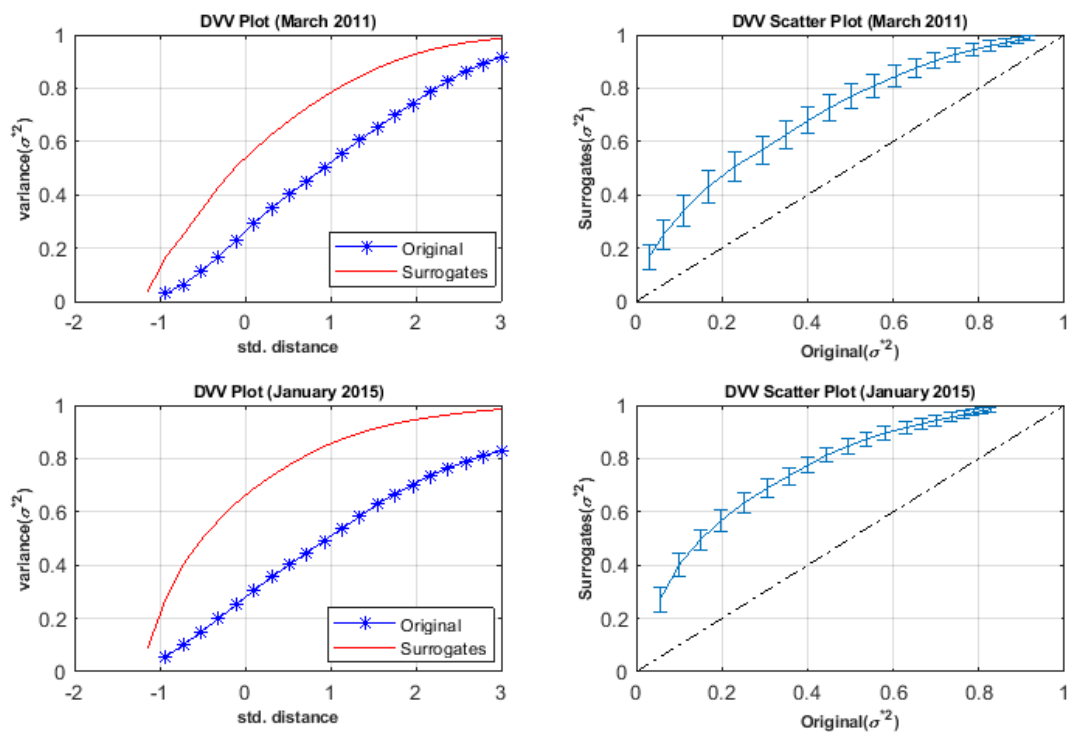


616

617 Figure 7: The DVV plot and Scatter plot during minor geomagnetic storm for January 2009 and
618 January 2014.

619

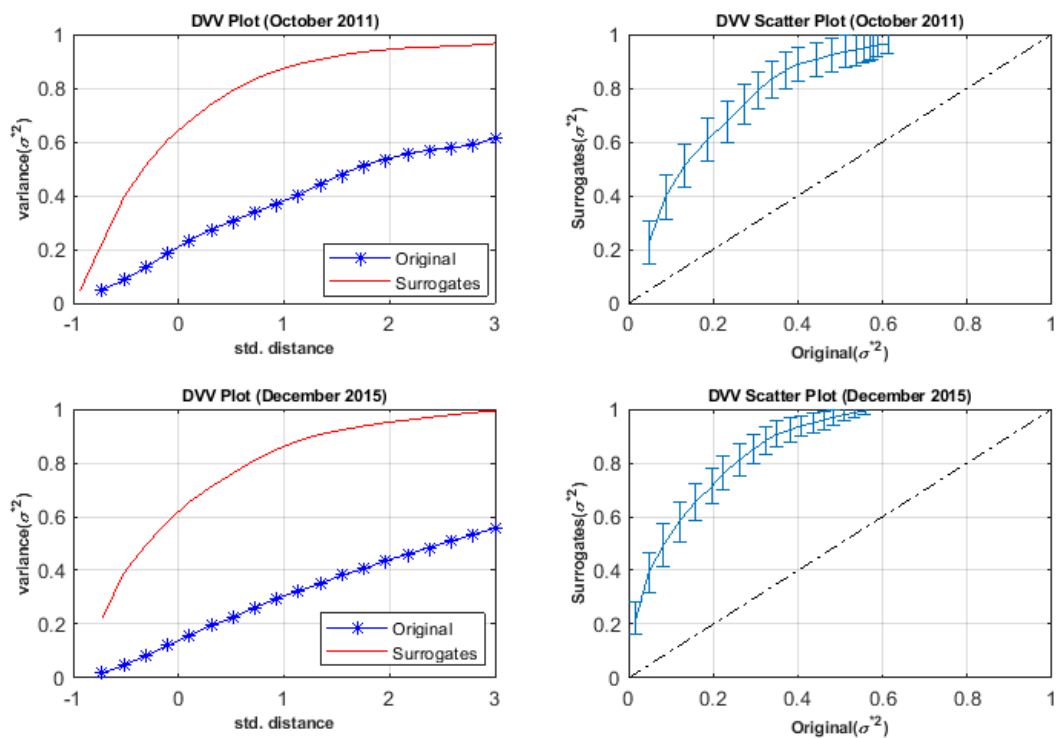
620



621

622 Figure 8: The DVV plot and Scatter plot during moderate geomagnetic storm for March 2011 and
623 January 2015.

624



625

626 Figure 9: The DVV plot and Scatter plot during major geomagnetic storm for October 2011 and
627 December 2015.

628

629